

Article

The Influence of 1 wt.% Cr on the Corrosion Resistance of Low-Alloy Steel in Marine Environments

Jianzhuo Gao ^{1,*}, Ningxi Wang ¹, Hui Chen ² and Xuexu Xu ^{3,*}¹ Beijing Institute of Metrology, Beijing 100029, China² School of Materials and Environmental Engineering, Shenzhen Polytechnic, Shenzhen 518055, China³ School of Materials Science and Engineering, China University of Petroleum (East China), Qingdao 266580, China

* Correspondence: gaojz@bjjl.cn (J.G.); 20230006@upc.edu.cn (X.X.)

Abstract: In this study, the effects of 1 wt.% Cr addition on the corrosion behavior and mechanisms of low-alloy structural steel in a marine environment were investigated through immersion experiments, corrosion product analysis, and electrochemical experimental systems. The results demonstrate that the addition of 1 wt.% Cr significantly enhances the corrosion resistance of low-alloy steel in marine environments. The influence of Cr addition on the corrosion product layer was analyzed through rust layer morphology, cross-sectional morphology, elemental distribution, and electrochemical systems. Cr addition effectively promotes the densification of the corrosion product layer on the surface of low-alloy steel in marine environments, hindering the penetration of corrosive ions and thus improving corrosion resistance. This study's findings can promote the optimization of corrosion resistance in low-alloy steel in marine environments and enhance its application prospects in marine environments.

Keywords: low-alloy steel; marine corrosion; Cr; corrosion product layer



Citation: Gao, J.; Wang, N.; Chen, H.; Xu, X. The Influence of 1 wt.% Cr on the Corrosion Resistance of Low-Alloy Steel in Marine Environments. *Metals* **2023**, *13*, 1050. <https://doi.org/10.3390/met13061050>

Academic Editor: Hannu Hänninen

Received: 15 May 2023

Revised: 25 May 2023

Accepted: 29 May 2023

Published: 30 May 2023



Copyright: © 2023 by the authors. Licensee MDPI, Basel, Switzerland. This article is an open access article distributed under the terms and conditions of the Creative Commons Attribution (CC BY) license (<https://creativecommons.org/licenses/by/4.0/>).

1. Introduction

Low-alloy structural steel is widely used in various fields such as marine platforms and island reef construction due to its excellent performance, but it is prone to corrosion and premature structural failure during service under the influence of the marine corrosion environment [1–5]. Corrosion resistance as an important property of low-alloy structural steel has attracted widespread attention from scholars. Micro-alloying [6–8], as a mainstream method for material performance optimization, has been widely applied to corrosion resistance optimization work in recent years.

Cr [9–13], as a universally recognized primary corrosion-resistant element, has been the subject of extensive research. Studies have shown that Cr can shift the self-corrosion potential of the steel matrix positively, and when the Cr content is higher, a passive film can form. In marine environments, Cr in low-alloy steel mainly enriches the inner rust layer, and its presence can promote the formation of α -FeOOH, facilitating rust layer densification. Simultaneously, the synergistic addition of Cu with Ni and Cu can achieve better corrosion resistance. Łukaszczyk et al. [14] studied the electrochemical behavior of low-alloy Fe-Cr steel containing 3% and 5% Cr in a neutral Na_2SO_4 electrolyte. The results show that the corrosion product film is a bilayer structure, with an outer layer of iron oxide/hydroxide and an inner Cr oxide-rich layer. A lower Cr content (3%) has a good improvement effect on the corrosion resistance of Fe-Cr steel, which is consistent with the research results of most people [15–17]. However, Kashima et al. [18] found that at high Cl^- concentrations, low-alloy steel containing 1 wt.% Cr exhibited a higher corrosion rate than carbon steel, reducing its corrosion resistance and increasing the acidity of the solution, further decreasing the corrosion resistance. When the Cr content increased to 4 wt.%, the higher Cr content in the rust layer inhibited the hydrolysis reaction of Cr^{3+} and Fe^{3+} , alleviating the decline in pH at the rust layer/matrix interface and improving the

steel's corrosion resistance. Therefore, the role of Cr in the corrosion resistance of low-alloy steel in marine environments remains controversial, and the impact of Cr on rust layer structure is still unclear. As a result, it is necessary to conduct research on the effects of Cr addition on the corrosion behavior of low-alloy steel in marine environments.

In this paper, two types of low-alloy structural Fe-1 wt.% Ni-0.3 wt.% Cu-Cr steel with 0 wt.% Cr and 1 wt.% Cr were prepared using vacuum melting methods. By simulating the marine environment through indoor immersion experiments and employing techniques such as microstructure analysis, corrosion product analysis, corrosion kinetics, and electrochemical testing, the effects of 1 wt.% Cr on the microstructure and corrosion behavior and mechanisms of low-alloy steel in marine environments were investigated. The research findings are expected to provide a foundation for the design of novel corrosion-resistant steels.

2. Materials and Methods

Two types of low-alloy structural steel with different Cr contents were prepared using vacuum melting technology and labeled as #1 and #2, respectively. The chemical compositions of the two experimental steels are presented in Table 1. Apart from the Cr element being investigated, there were no significant differences in the contents of other elements, meeting the research requirements.

Table 1. Chemical composition of two low-alloy steels (wt.%).

Steel	C	Si	Mn	P	S	Ni	Cu	Cr
1#	0.044	0.52	1.22	0.0089	0.0021	0.98	0.31	-
2#	0.039	0.46	1.30	0.0085	0.0019	1.02	0.31	0.97

Samples measuring 10 mm × 10 mm × 3 mm were cut along the rolling direction of the steel plates using wire cutting for microstructure observation. The sample surfaces were sequentially ground with SiC abrasive paper up to 3000 grit, followed by polishing to a mirror finish. The samples were then rinsed with deionized water and ethanol and dried for further use. After etching the polished working surfaces for 5 s using a 4 vol.% nitric acid–ethanol solution, the samples were quickly rinsed with deionized water and ethanol and dried. The etched samples were observed under a Quanta 250 scanning electron microscope (SEM, FEI, Hillsboro, OR, USA) to investigate their microstructure, as shown in Figure 1. As can be seen from the figure, the microstructures of both experimental steels consist of a mixed structure of lath and granular bainite [19,20]. In Steel 1#, bainitic ferrite is predominant. With the addition of Cr, the amount of lath bainite in the steel increases, and the bainite grains are noticeably refined.

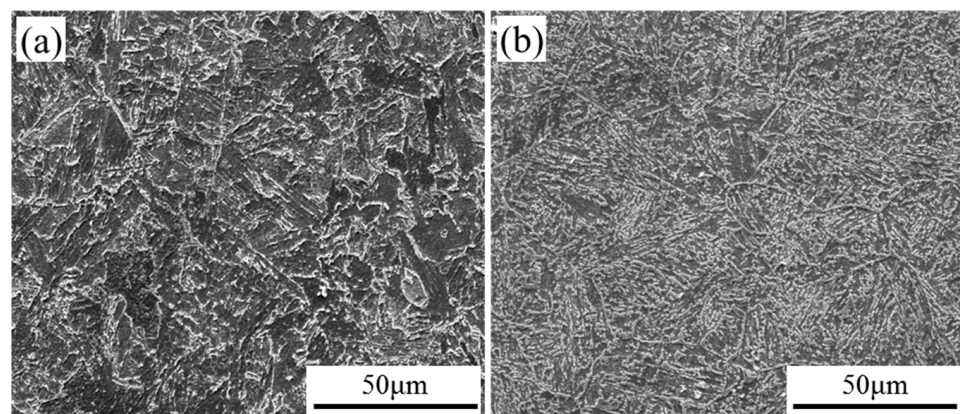


Figure 1. Microstructure of two low-alloy steels: (a) Steel 1# and (b) Steel 2#.

Immersion tests were carried out to simulate the marine environment, with plate-shaped samples measuring 50 mm × 25 mm × 3 mm cut along the rolling direction. The samples were polished to 1200 grit, cleaned sequentially with ultrapure water and ethanol, and dried before weighing and measuring their dimensions. The immersion solution was a simulated seawater with the composition ratios shown in Table 2. The immersion tests were conducted over periods of 7, 15, and 30 days. To improve the accuracy of the experiment, three parallel samples were prepared for each type of experimental steel for each test period.

Table 2. Chemical composition of the simulated seawater, data from [21], g/L.

NaCl	MgCl ₂	Na ₂ SO ₄	CaCl ₂	KCl	NaHCO ₃	KBr	H ₃ BO ₃	SrCl ₂	NaF
24.53	5.20	4.09	1.16	0.695	0.201	0.101	0.027	0.025	0.003

After each test period, the samples were derusted using a rust removal solution consisting of 500 mL water, 500 mL hydrochloric acid, and 3.6 g hexamethylenetetramine. The samples were then rinsed with deionized water and ethanol, dried, weighed, and the corrosion rate was calculated. The calculation formulas for corrosion loss and corrosion rate were the same as those in references [22–25]:

$$w = \frac{m_0 - m_t}{S} \quad (1)$$

$$v = \frac{(m_0 - m_t) \times 10^4}{S\rho t} \quad (2)$$

where w is the corrosion weight loss (g/cm²), v is the corrosion rate (mm/y), m_0 is the original weight of the sample (g), m_t is the weight of the sample after rust removal (g), S is the exposure area of the sample (cm²), ρ is the density of steel (7.8 g/cm³), and t is the exposure time (h).

The surface and cross-sectional morphologies of the rust layers of both experimental steels after different immersion periods were observed using an SEM, and the elemental distribution of the rust layer cross-sections was analyzed using EDS. The rust layers scraped from the surfaces of the samples at different periods were ground into powders using a quartz mortar for subsequent rust layer composition analysis. X-ray diffraction (XRD) was employed to analyze the phase composition of the rust layers of the two experimental steels after different immersion periods, with working voltage and current set at 40 kV and 150 mA [26], respectively. The scanning rate was 3°/min, and the diffraction angle scanning range was 10° to 90°. A 3D analysis of the surface corrosion morphology after derusting was performed using a laser confocal microscope.

Electrochemical tests were conducted on the rust layers after immersion using a traditional three-electrode system, with the rusted samples serving as the working electrode, a platinum plate as the auxiliary electrode, and a saturated calomel electrode as the reference electrode. The electrochemical test solution was simulated seawater. Electrochemical tests were carried out on a 3F electrochemical workstation (Princeton, San Diego, CA, USA). The frequency test range for the alternating current impedance was 100 kHz to 10 mHz [21,27], and the excitation potential amplitude of the alternating current impedance test was 10 mV. After testing, the data were analyzed using Zsimp Win software (3.5, Ann Arbor, MI, USA). All electrochemical tests were conducted at room temperature, and each test was performed three times to ensure the reliability of the results.

3. Result

3.1. Corrosion Rate Analysis

Figure 2 shows the corrosion loss of the two types of low-alloy steel samples after immersion corrosion tests. As seen in the figure, the corrosion loss of both materials

increases gradually with the progression of the corrosion cycle. With the addition of Cr element in Steel #2, the corrosion weight loss of Steel #2 at 7 days is slightly lower than that of Steel #1, but the difference is small. As the soaking time increases to 15 and 30 days, the gap in corrosion weight loss between Steel #2 and Steel #1 becomes larger, indicating that the addition of Cr can effectively inhibit the corrosion of low-alloy steel in a marine environment, thus reducing the corrosion weight loss of Steel #2. From the perspective of corrosion weight loss, the difference in weight loss between the two types of steel is not significant. Therefore, the corrosion rate of the two types of experimental steel soaked for different times is calculated using Equation (2) to more intuitively characterize the effect of Cr addition on the corrosion behavior of low-alloy steel. The calculation results are shown in Figure 3. It can be observed that as the immersion time increases from 7 to 15 days, the corrosion rates of both experimental steels exhibit a significant decreasing trend, with the corrosion rate of Steel 2# being noticeably lower than that of Steel 1#. As the immersion time increases from 15 to 30 days, the corrosion rate rises again, but the increase in the corrosion rate of Steel 2# is lower compared to Steel 1#, suggesting that the corrosion product layer on the steel surface is not dense enough for long-term immersion, leading to intensified material corrosion. At the same time, the addition of Cr promotes the densification of the corrosion product layer, thereby reducing the corrosion rate.

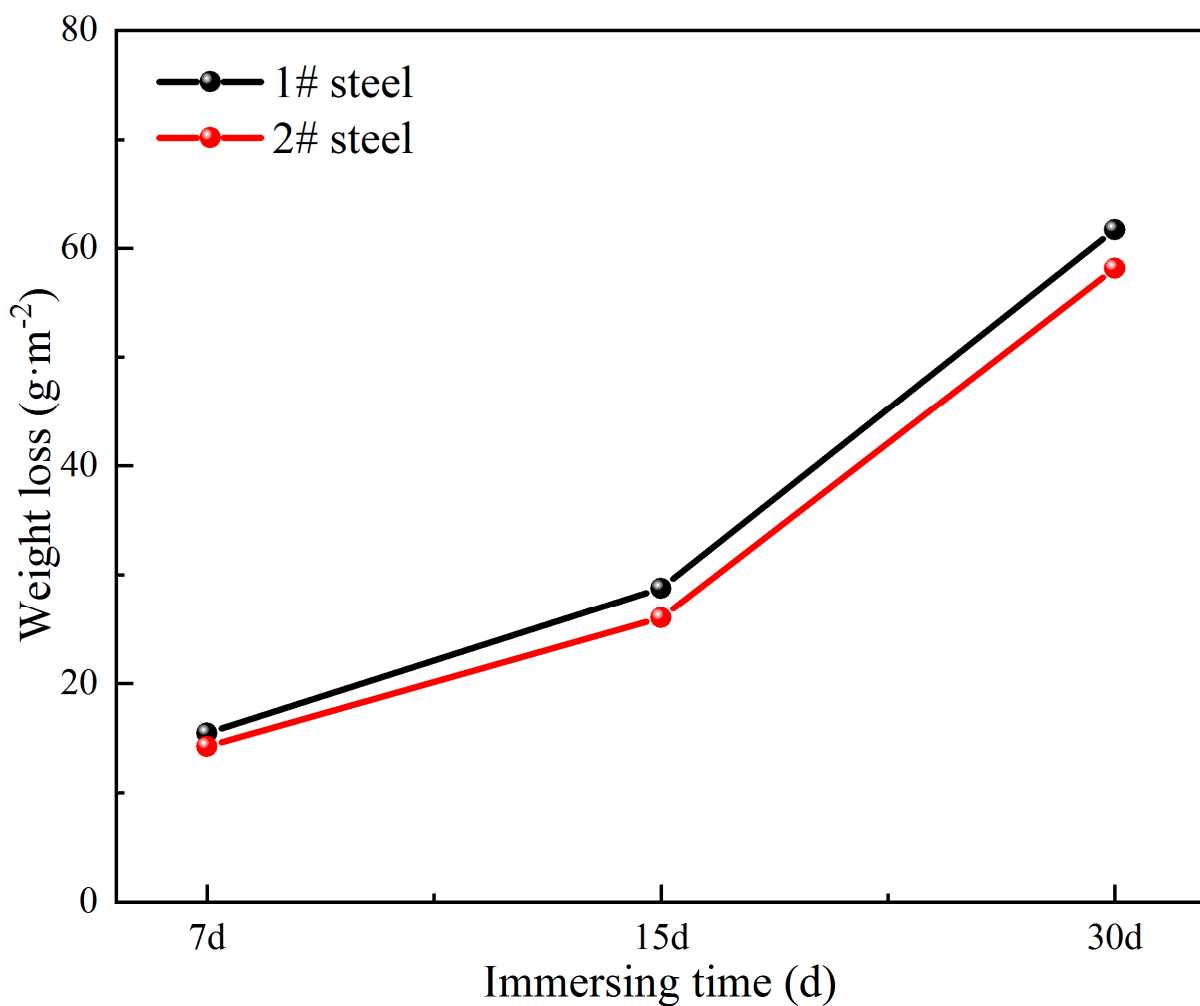


Figure 2. Corrosion weight loss of two low-alloy steels in a simulated seawater environment.

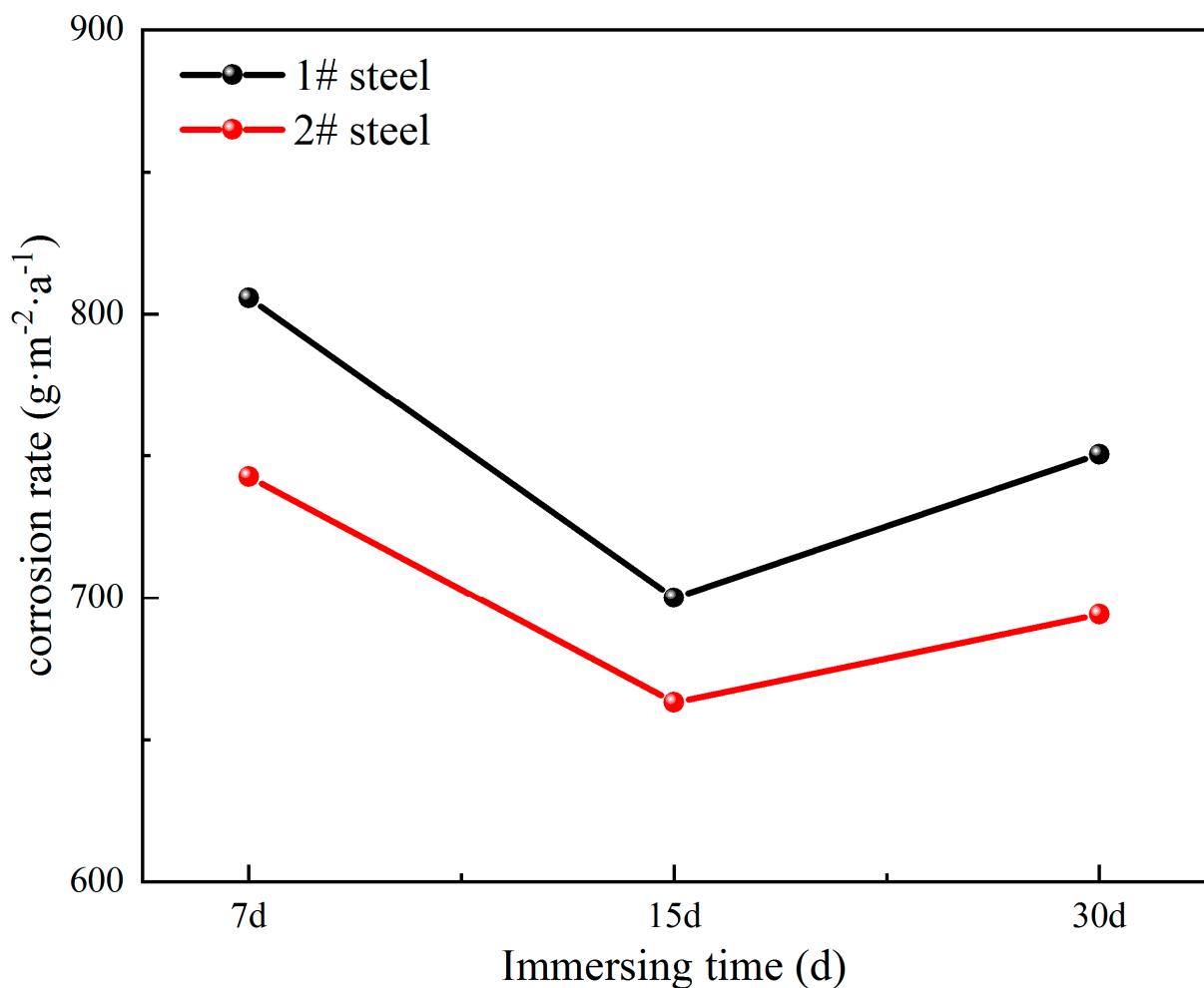


Figure 3. Corrosion rates of two low-alloy steels in a simulated seawater environment.

3.2. Evolution of Corrosion Products

To further analyze the influence of Cr addition on the corrosion behavior of low-alloy steel, the microscopic morphology of the rust layer surfaces of the two materials after immersion for different periods was examined. Figure 4 shows the rust layer morphology of the sample surfaces after 7 days of immersion. It can be seen that after 7 days of immersion, both experimental steels exhibit evident corrosion product attachment on the surface. Steel 1# has a large amount of granular corrosion products, while Steel 2# has fewer granular corrosion products. Upon closer examination, it was found that the corrosion product layer of Steel 1# is relatively loose, whereas the corrosion product layer of Steel 2# is denser. The degree of compactness of the rust layer surface represents whether it can provide a pathway for the transport of the corrosive medium during the corrosion process and, to a certain extent, reflects the protective nature of the rust layer. Therefore, from the rust layer morphology observed after 7 days, the rust layer structure of Steel 2# provides better protection for the steel substrate.

The surface rust layer morphology of the experimental steels after 30 days of immersion was observed, as shown in Figure 5. It can be seen that after 30 days of immersion, the size of the granular corrosion products on steel 1# increases, and the steel surface does not form a dense and continuous corrosion product layer. In contrast, no large-sized granular corrosion products are evident on the surface of Steel 2#. Closer examination reveals the presence of tiny granular corrosion products adhering to the surface, forming a relatively dense corrosion product layer. However, numerous cracks were observed in the corrosion product layer of Steel 2#, indicating that the addition of 1 wt.% Cr promotes the formation

of a dense corrosion product layer, but the layer still exhibits cracks, providing a pathway for the penetration of corrosion ions. This result also explains the phenomenon of improved corrosion resistance with the addition of Cr but the continued increase in corrosion rate over an extended period.

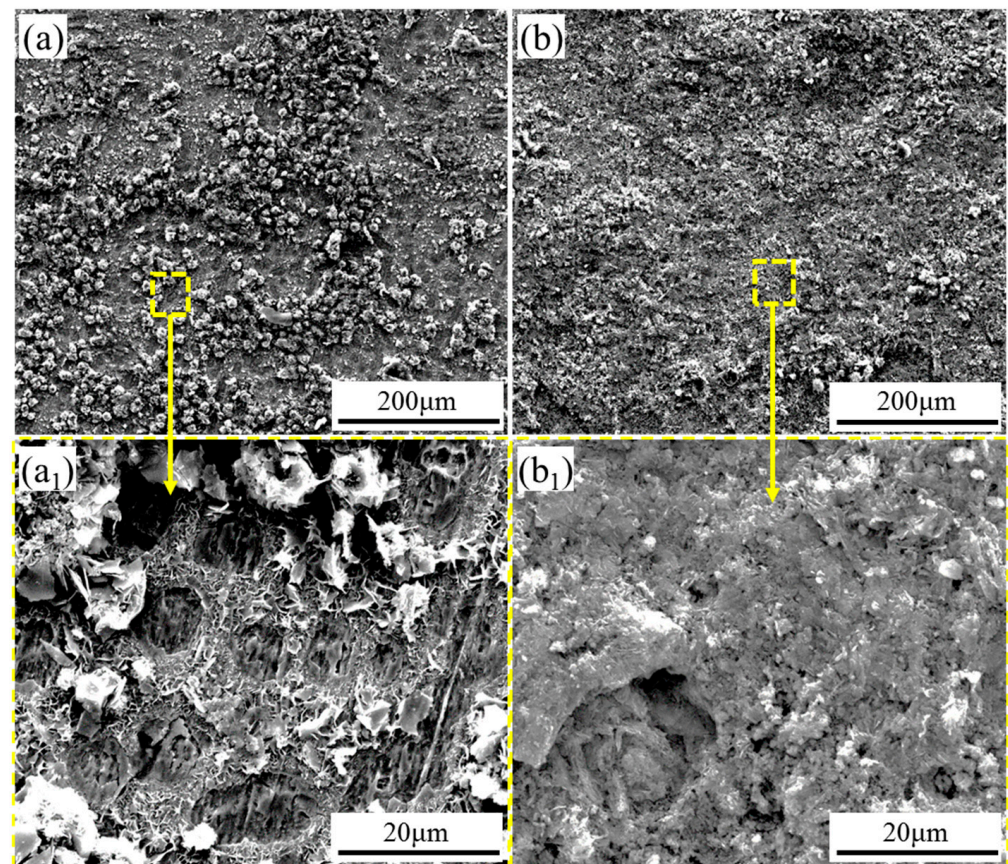


Figure 4. Surface morphology and magnified local views of two low-alloy steels after immersion in a simulated seawater environment for 7 days: (a), (a₁) Steel 1# and (b), (b₁) Steel 2#. (The yellow frame indicates the local area and its magnified image.)

After the immersion experiment, the cross-sectional morphology and elemental distribution of the rust layers of the two experimental steels after 30 days of immersion were observed, as shown in Figure 6. It can be seen from the figure that the rust layer of Steel 1# is relatively loose and porous, while the rust layer of Steel 2# is denser. Notably, significant cracks were found in the rust layer of Steel 2#, which is consistent with the rust layer surface morphology results in Figure 5. From the elemental distribution results, it can be observed that the rust layer of Steel 1# exhibits enrichment of O and Cl, whereas with the addition of Cr, the rust layer of Steel 2# shows a significant enrichment of Cr elements without Cl enrichment, indicating that the addition of Cr can form a dense corrosion product layer, thereby hindering the penetration of corrosive Cl ions and reducing the corrosion rate of experimental steel in the marine environment.

XRD was employed to analyze the phase composition of the rust layers of the two experimental steels after immersion for different periods, and the results are shown in Figure 7. It can be seen that the phase composition of the rust layers of the two experimental steels is essentially consistent, mainly consisting of Fe_3O_4 , $\alpha\text{-FeOOH}$, $\gamma\text{-FeOOH}$, CaCO_3 , and Fe. The CaCO_3 peak is mainly due to the deposition of CaCO_3 from the experimental solution on the rust layer surface during the drying process, rather than being a component of the rust layer phase. As the immersion time increases, no significant changes occur in the phase types of the two experimental steels, but the peak intensity and width of

each steel's XRD differ, indicating that the addition of Cr can affect the proportion of each phase. The XRD results were semi-quantitatively analyzed using the relative intensity ratio method [28], and the results are shown in Figure 8. It can be seen that the main composition phase of the rust layers of the two experimental steels after corrosion in the marine environment for different periods is Fe_3O_4 . The Fe_3O_4 content in Steel 1# increases with the corrosion time. With the addition of Cr, the α -FeOOH content of Steel 2# begins to increase, and the Fe_3O_4 content gradually decreases. γ -FeOOH is considered an initial rust layer product, exhibiting strong reactivity and relatively loose structure; its presence is unfavorable for rust layer structure stability. Compared to γ -FeOOH, Fe_3O_4 has higher stability and a relatively denser structure, but it possesses strong electrical conductivity and is easily reduced. α -FeOOH is a thermodynamically stable phase that can effectively enhance the rust layer's stability. Therefore, the α/γ^* is commonly used to evaluate the protective performance of the corrosion product layer in the marine environment, where α represents the content of α -FeOOH, and γ^* represents the total content of Fe_3O_4 and γ -FeOOH. As seen in Figure 8, as the immersion time increases, the α/γ^* of Steel 1# gradually decreases, while that of Steel 2# gradually increases, indicating that the addition of Cr significantly improves both the protective and stability properties of the rust layer.

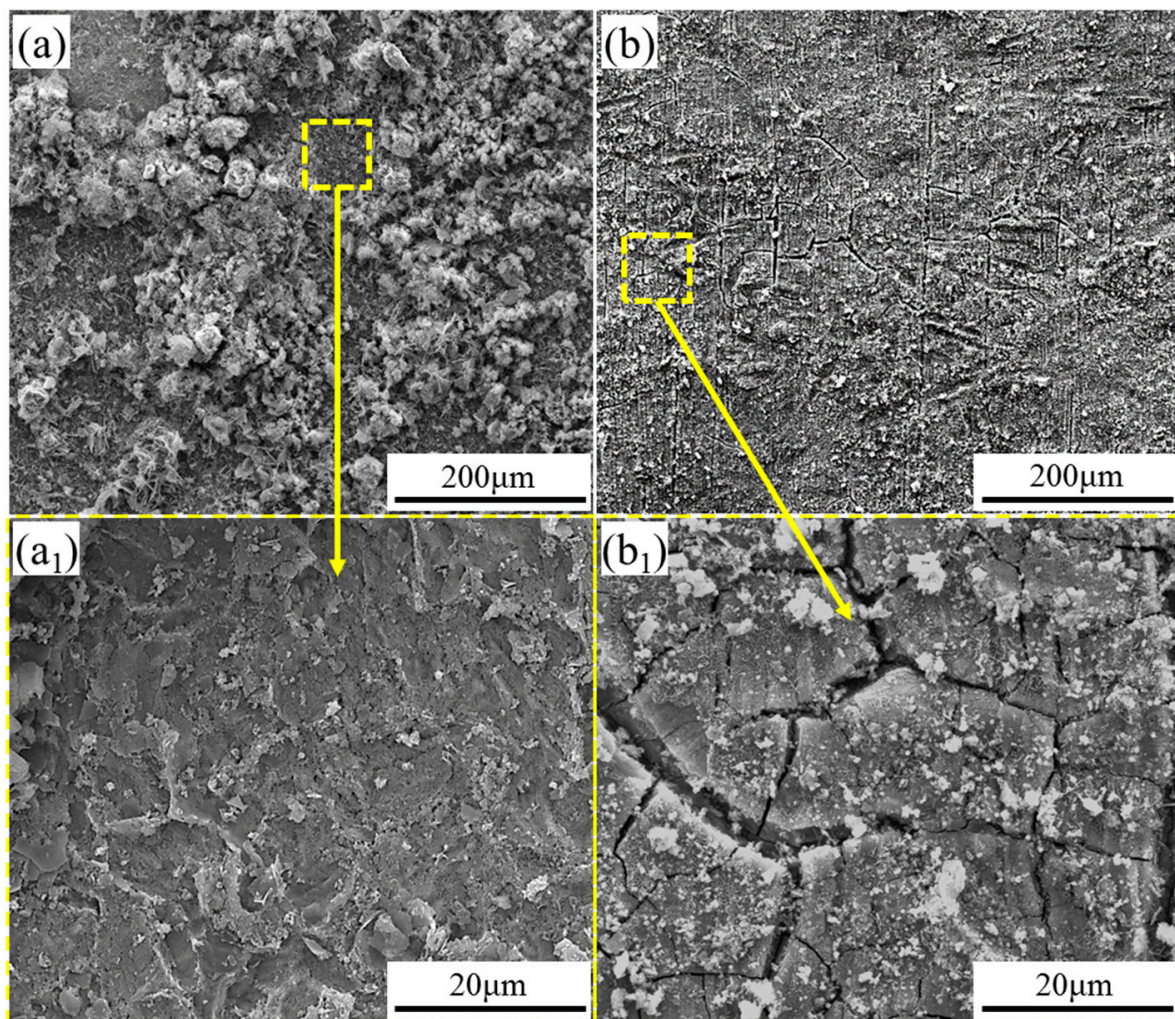


Figure 5. Surface morphology and magnified local views of two low-alloy steels after immersion in a simulated seawater environment for 30 days: (a), (a₁) Steel 1# and (b), (b₁) Steel 2#. (The yellow frame indicates the local area and its magnified image.)

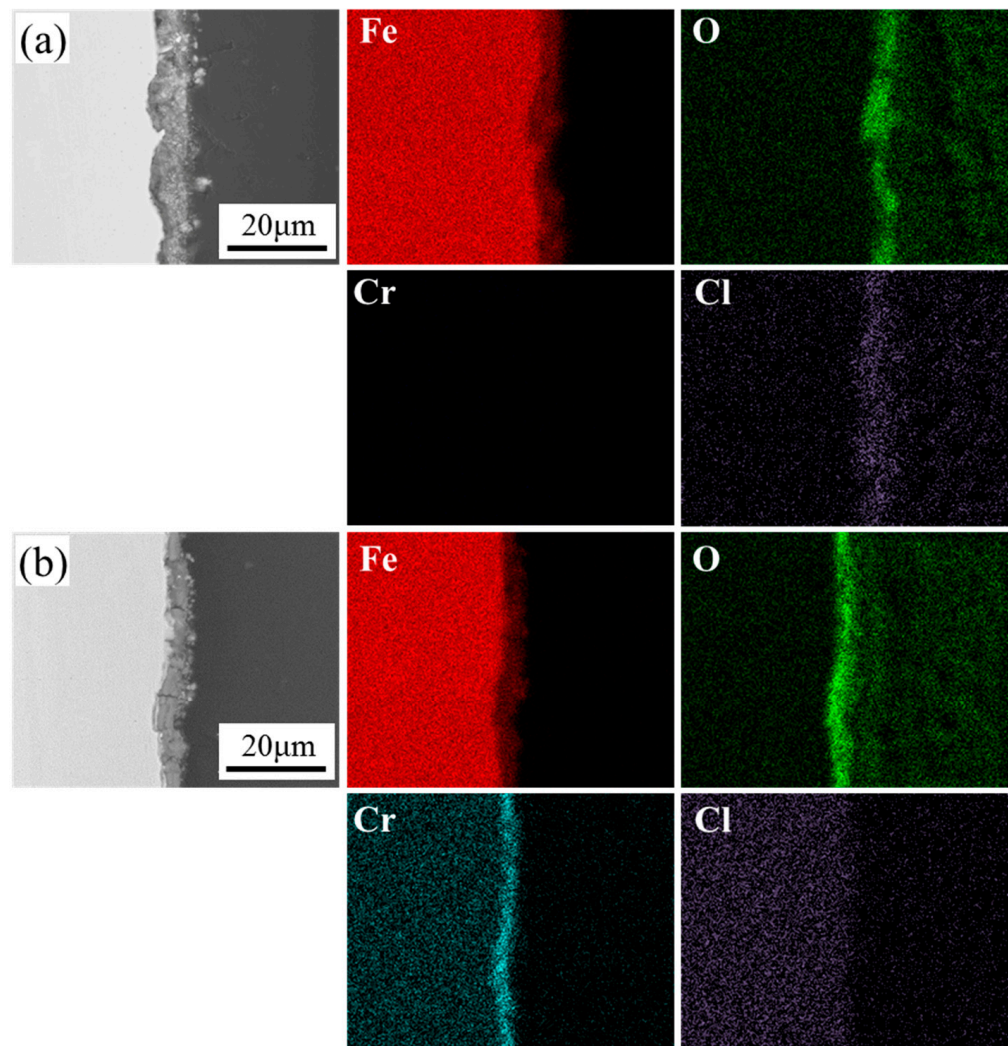


Figure 6. Cross-sectional morphology and elemental distribution of two low-alloy steels after immersion for 30 days: (a) Steel 1# and (b) Steel 2#.

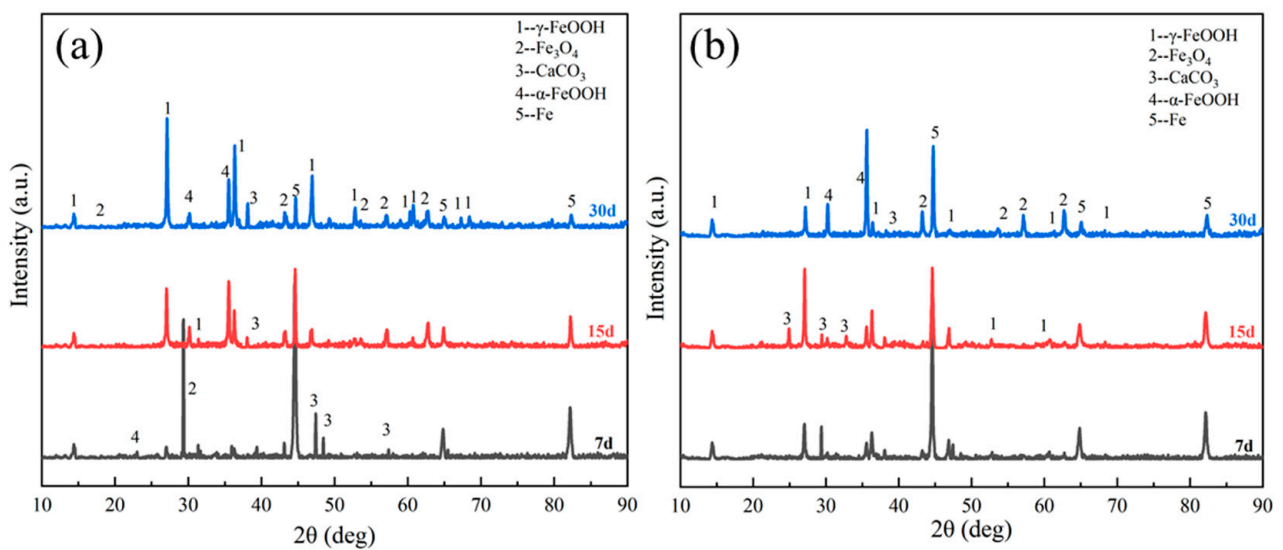


Figure 7. Phase composition of the rust layers of two low-alloy steels after immersion experiments: (a) Steel 1# and (b) Steel 2#.

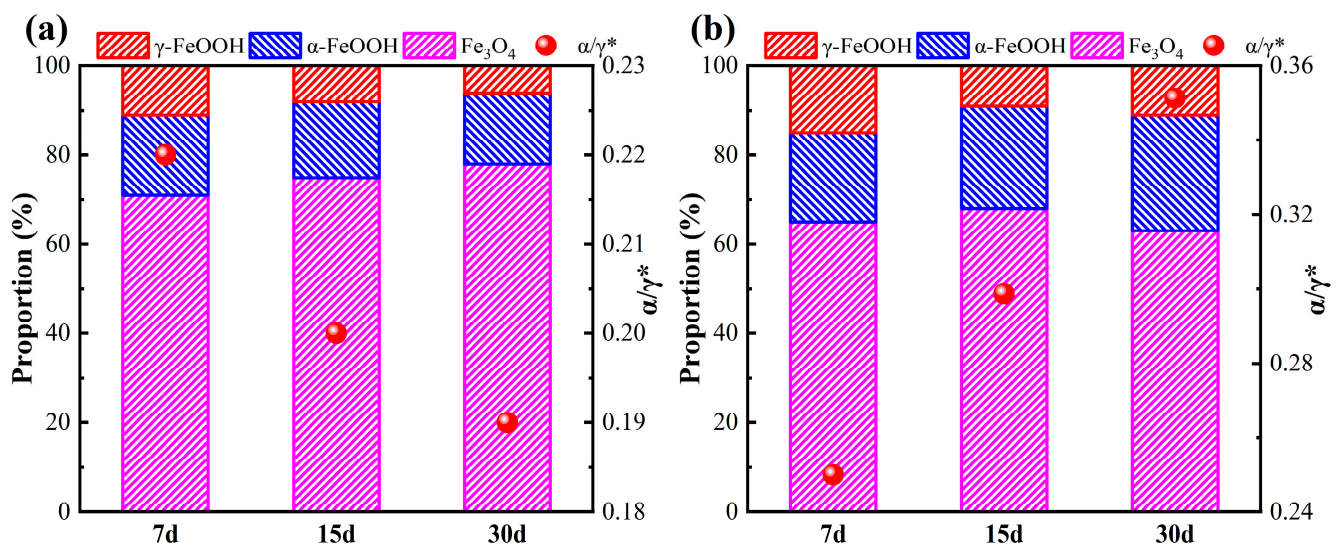


Figure 8. Phase proportions and α/γ^* values of rust layers of two low-alloy steels after immersion experiments: (a) Steel 1# and (b) Steel 2#.

3.3. Corrosion Morphology Analysis

To further analyze the corrosion behavior of the two experimental steels in the marine environment, laser confocal technology was employed to characterize the 3D morphology of the two experimental steels after removing the corrosion product layer for different immersion periods, as shown in Figure 9. It can be seen from the figure that as the immersion time increases, the local corrosion of both experimental steels intensifies. After 7 days of immersion, Steel 1# exhibits significant pitting traces, while Steel 2# shows no obvious pitting. As the immersion time increases, the number and depth of the pits in Steel 1# increase, indicating that local corrosion beneath the rust layer of Steel 1# becomes more pronounced under long-term immersion. After 30 days of immersion, Steel 2# also shows a small number of pits and local corrosion traces, indicating that although the addition of Cr promotes densification of the rust layer, it still leads to localized corrosion traces due to acidification beneath the rust layer. This is consistent with the previously discussed rust layer cross-sectional morphology results.

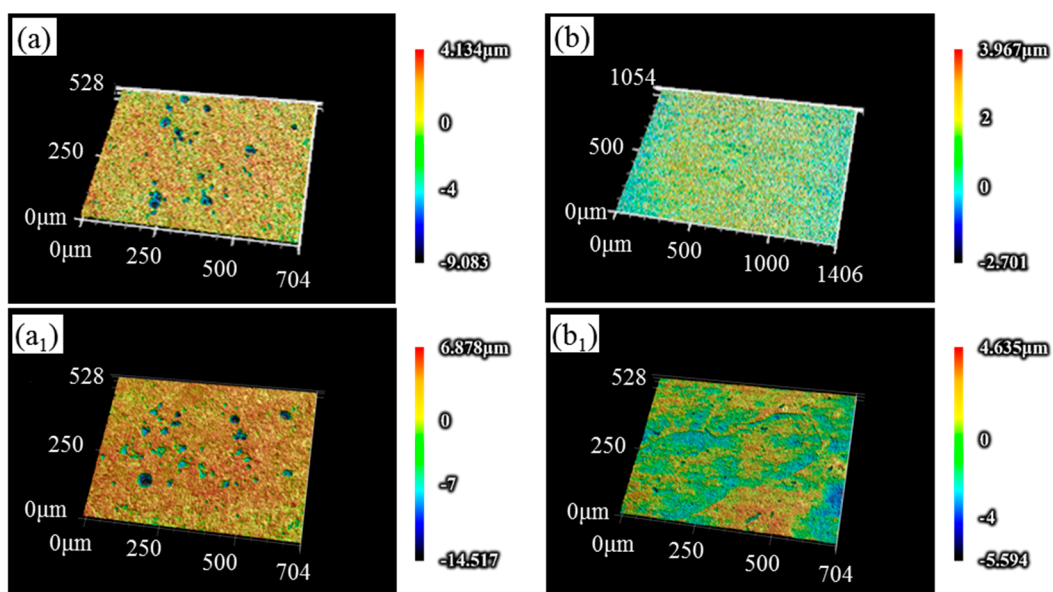


Figure 9. The 3D corrosion morphologies of two low-alloy steels after different immersion periods with rust layers removed: (a) Steel 1#—7 d, (a1) Steel 1#—30 d, (b) Steel 2#—7 d, and (b1) Steel 2#—30 d.

3.4. Electrochemical Analysis

Research has shown that electrochemical impedance spectroscopy (EIS) is an effective approach to evaluate the protective properties of low-alloy steel rust layers. Therefore, the electrochemical impedance of the two experimental steels in the marine environment after different immersion periods was measured, and the results are shown in Figure 10. It can be seen that the curve shapes of both experimental steels after different immersion times are similar, indicating that the addition of Cr does not change the electrochemical mechanism of low-alloy steel. As the immersion time increases, the capacitance arc radius of both experimental steels after 7 days of immersion is relatively small. As the immersion time extends to 15 days, the capacitance arc radius increases, and when immersed for 30 days, the capacitance arc radius increases significantly, suggesting that a protective rust layer forms on the steel surface as corrosion progresses, and the capacitance arc radius can be used to compare the protective properties of rust layers. The EIS results were simulated using the equivalent circuit diagram shown in Figure 11 to quantitatively evaluate the protective properties of the rust layer, with fitting results presented in Table 3. R_s represents the solution resistance, Q_f and R_p are the constant phase angle elements and pore resistance of the rust layer, and Q_{dl} and R_{ct} represent the constant phase angle element and charge transfer resistance of the double layer at the matrix interface, respectively.

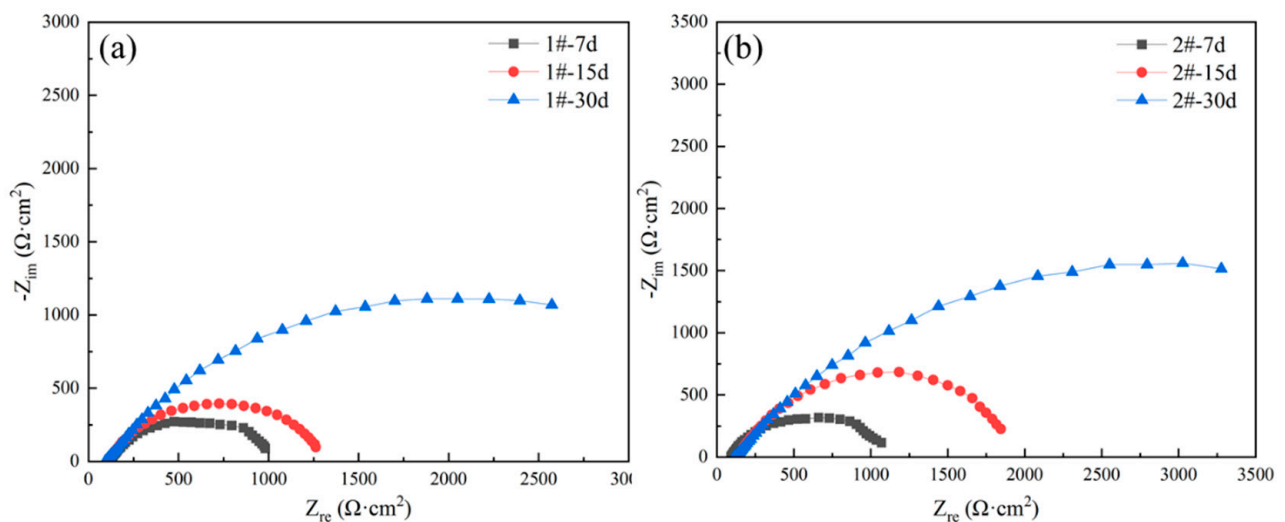


Figure 10. EIS analysis of two low-alloy steels in a simulated seawater environment after immersion experiments: (a) Steel 1# and (b) Steel 2#.

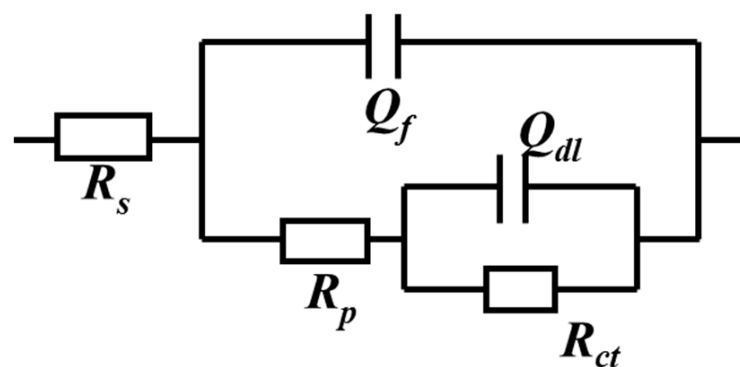


Figure 11. Equivalent circuit diagrams of EIS for two experimental steels after immersion experiments.

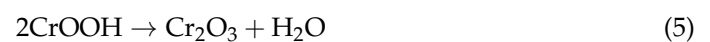
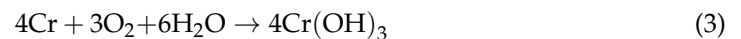
Table 3. Impedance spectrum fitting results of two low-alloy steels.

	R_s ($\Omega \cdot \text{cm}^2$)	$Q_f \times 10^{-4}$ ($\Omega \text{ cm}^{-2} \text{ s}^{n_1}$)	n_1	R_p ($\Omega \cdot \text{cm}^2$)	$Q_{dl} \times 10^{-4}$ ($\Omega \text{ cm}^{-2} \text{ s}^{n_2}$)	n_2	R_{ct} ($\Omega \cdot \text{cm}^2$)	$\chi^2 \times 10^{-4}$
1#—7 d	113.7	8.64	0.74	205.8	3.61	0.69	715	3.48
1#—15 d	106.5	6.58	0.72	262	5.14	0.72	980	1.42
1#—30 d	95.22	9.12	0.64	615	6.23	1	1978	2.26
2#—7 d	92.88	1.25	0.74	221.2	4.71	0.75	825.1	4.20
2#—15 d	130.4	4.56	0.76	261.8	2.37	0.77	1341	3.08
2#—30 d	128.6	3.46	0.87	720.7	8.01	0.64	2881	1.28

From the Table 3, it can be observed that the R_p of both steel samples increases with the immersion time, indicating that the rust layers of both steels gradually densify over time, providing some protection to the steel substrate. The addition of 1 wt.% Cr results in a higher increase in R_p , indicating that the improvement effect on the corrosion product layer is more pronounced after the addition of Cr. As Cr is added, R_{ct} gradually increases, suggesting that the rust layer formed by Steel 2# offers better protection, effectively hindering the migration of corrosive ions to the interface between the rust layer and steel substrate, resulting in a hindered interface charge transfer process. In addition, it can be seen from Table 3 that the χ^2 value of the two fittings are both in the order of 10^{-4} , meaning that the circuit has a better fitting quality.

4. Discussion

Research [29,30] has shown that low-alloy steel undergoes dissolution as the anode in electrochemical reactions, during which Cr dissolves to form $\text{Cr}(\text{OH})_3$, which then gradually dehydrates during the drying process to form Cr_2O_3 . The related reactions are as follows:



Studies by Sun et al. [31,32] indicate that the dissolved Cr^{3+} in the rust layer can replace some of the Fe^{3+} positions in $\alpha\text{-FeOOH}$, thereby forming Cr-doped $\alpha\text{-(Fe, Cr)OOH}$. Some Cr can also occupy the Fe^{3+} positions in Fe_3O_4 to form FeCr_2O_4 . Due to the higher stability of Cr^{3+} compared to Fe^{3+} , the structure and thermodynamic stability of Cr-doped FeCr_2O_4 and $\alpha\text{-(Fe, Cr)OOH}$ are enhanced, reducing the risk of being reduced to $\gamma\text{-FeOOH}$ and improving the stability of the rust layer. Combining the XRD analysis results, it is known that the addition of 1 wt.% Cr promotes the conversion of $\gamma\text{-FeOOH}$ to $\alpha\text{-FeOOH}$ and Fe_3O_4 , enhancing the stability of the rust layer and inhibiting the infiltration of corrosive ions. At the same time, the addition of Cr also promotes the formation of oxidation products such as Cr_2O_3 , CrO_3 , and $\text{Cr}(\text{OH})_3$, which, except for CrO_3 , all exhibit excellent stability and corrosion resistance. From the cross-sectional morphology of the rust layer, it is evident that there is a significant enrichment of Cr in the corrosion product layer after Cr addition, indicating that the content of Cr-containing products in the rust layer significantly increases with Cr addition, which in turn implies an increase in the rust layer's protective and stability properties.

Therefore, the main effect of Cr addition on the improvement of corrosion resistance of low-alloy steel in the marine environment is reflected in the optimization of the corrosion product layer. On one hand, with the addition of Cr, the corrosion product layer becomes denser, with fewer defects in the rust layer compared to Steel 1# and fewer channels for the corrosive medium. On the other hand, the enrichment of Cr in the corrosion product layer

endows the rust layer with cation-selective permeability, making it difficult for corrosive ions to penetrate the steel substrate.

5. Conclusions

In this study, two low-alloy structural Fe-1 wt.% Ni-0.3 wt.% Cu-Cr steels with 0 wt.% Cr and 1 wt.% Cr content were prepared using vacuum melting technology. The effects of Cr on the microstructure and corrosion behavior and mechanisms of low-alloy steel in the marine environment were analyzed through microstructure observation, immersion corrosion experiments, corrosion product analysis, and electrochemical testing. The main conclusions are as follows:

- (1) The addition of Cr can change the microstructure, promoting the transformation from granular bainite to lath bainite;
- (2) The addition of Cr can effectively reduce the corrosion rate of low-alloy structural steel in the marine environment;
- (3) The addition of Cr can promote the formation of stable α -FeOOH in the rust layer, improve the loose and porous structure of the corrosion product layer, promote the densification of the rust layer, and effectively hinder the infiltration of corrosive ions;
- (4) The improvement effect of 1 wt.% Cr on the rust layer is limited, as the corrosion product layer still has obvious cracks. Further research is needed to better optimize the corrosion product layer structure and inhibit the corrosion of low-alloy steel in the marine environment.

Author Contributions: Conceptualization and writing—original draft: J.G. Validation: N.W. Investigation: H.C. Writing—original draft and writing—review and editing: X.X. All authors have read and agreed to the published version of the manuscript.

Funding: This research received no external funding.

Data Availability Statement: The raw/processed data required to reproduce these findings cannot be shared at this time as the data are related to an ongoing study.

Conflicts of Interest: The authors declare no conflict of interest.

References

1. Southwell, C.; Forgeson, B.; Alexander, A. Corrosion of Metals in Tropical Environments (Part 2—Atmospheric Corrosion of Ten Structural Steels). *Corrosion* **1958**, *14*, 55–59. [\[CrossRef\]](#)
2. Dong, B.; Liu, W.; Chen, L.; Zhang, T.; Fan, Y.; Zhao, Y.; Li, S.; Yang, W.; Banthukul, W. Optimize Ni, Cu, Mo element of low Cr-steel rebars in tropical marine atmosphere environment through two years of corrosion monitoring. *Cem. Concr. Compos.* **2022**, *125*, 104317. [\[CrossRef\]](#)
3. Zhang, Y.; Jin, S.; Jiang, C.; Yang, J.J.; Sha, G. Formation of high-temperature inner oxide scale on low alloy steels: Segregation, partitioning and transformation reactions. *Corros. Sci.* **2022**, *195*, 109980. [\[CrossRef\]](#)
4. Sun, Y.P.; Wei, X.; Dong, J.H.; Chen, N.; Zhao, H.Y.; Ren, Q.Y.; Ke, W. Understanding the role of alloyed Ni and Cu on improving corrosion resistance of low alloy steel in the simulated Beishan groundwater. *J. Mater. Sci. Technol.* **2022**, *130*, 124–135. [\[CrossRef\]](#)
5. Liu, Z.; Wang, Y.; Zhai, Y.; Qiao, Y.; Zheng, C.; Wang, D.; Shi, X.; Lu, H.; Liu, C. Corrosion behavior of low alloy steel used for new pipeline exposed to H₂S-saturated solution. *Int. J. Hydrog. Energy* **2022**, *47*, 33000–33013. [\[CrossRef\]](#)
6. Xu, X.X.; Zhang, T.Y.; Wu, W.; Jiang, S.; Yang, J.W.; Liu, Z.Y. Optimizing the resistance of Ni-advanced weathering steel to marine atmospheric corrosion with the addition of Al or Mo. *Constr. Build. Mater.* **2021**, *279*, 122341. [\[CrossRef\]](#)
7. Konishi, H.; Yamashita, M.; Uchida, H.; Jun, M. Characterization of rust layer formed on Fe, Fe-Ni and Fe-Cr alloys exposed to Cl-rich environment by Cl and Fe K-Edge XANES measurements. *Mater. Trans.* **2005**, *46*, 329–336. [\[CrossRef\]](#)
8. Mizoguchi, T.; Ishii, Y.; Okada, T.; Kimura, M.; Kihira, H. Magnetic property based characterization of rust on weathering steels. *Corros. Sci.* **2005**, *47*, 2477–2491. [\[CrossRef\]](#)
9. Kamimura, T.; Stratmann, M. The influence of chromium on the atmospheric corrosion of steel. *Corros. Sci.* **2001**, *43*, 429–447. [\[CrossRef\]](#)
10. Yuan, R.; Wu, H.B.; Gu, Y. Effect of alloyed Cr on corrosion behavior of low-alloy steel in wet atmosphere. *Mater. Corros.-Werkst. Korros.* **2022**, *73*, 918–931. [\[CrossRef\]](#)
11. Yang, X.J.; Yang, Y.; Sun, M.H.; Jia, J.H.; Cheng, X.Q.; Pei, Z.B.; Li, Q.; Xu, D.; Xiao, K.; Li, X.G. A new understanding of the effect of Cr on the corrosion resistance evolution of weathering steel based on big data technology. *J. Mater. Sci. Technol.* **2022**, *104*, 67–80. [\[CrossRef\]](#)

12. Park, J.S.; Kim, S.O.; Jeong, Y.J.; Lee, S.G.; Choi, J.K.; Kim, S.J. Long-Term Corrosion Behavior of Strong and Ductile High Mn-Low Cr Steel in Acidic Aqueous Environments. *Materials* **2022**, *15*, 1746. [[CrossRef](#)]
13. Gupta, K.K.; Haratian, S.; Ambat, R. On CO₂ corrosion resistance of low carbon steels in the formation water chemistry: The impact of Cr content as an alloying element. In Proceedings of the 18th Nordic Corrosion Congress, Turku, Finland, 31 May–2 June 2022.
14. Lukaszczyk, A.; Banaś, J.; Pisarek, M.; Seyeux, A.; Marcus, P.; Światowska, J. Effect of Cr Content on Corrosion Resistance of Low-Cr Alloy Steels Studied by Surface and Electrochemical Techniques. *Electrochem* **2021**, *2*, 546–562. [[CrossRef](#)]
15. Song, D.; Hao, J.; Yang, F.L.; Chen, H.D.; Liang, N.N.; Wu, Y.Y.; Zhang, J.C.; Ma, H.; Klu, E.E.; Gao, B.; et al. Corrosion behavior and mechanism of Cr-Mo alloyed steel: Role of ferrite/bainite duplex microstructure. *J. Alloys Compd.* **2019**, *809*, 151787. [[CrossRef](#)]
16. Zhang, S.H.; Bian, T.T.; Mou, L.M.; Yan, X.Y.; Zhang, J.L.; Zhang, Y.Z.; Liu, B.S. Alloy design employing Ni and Mo low alloying for 3Cr steel with enhanced corrosion resistance in CO₂ environments. *J. Mater. Res. Technol.* **2023**, *24*, 1304–1321.
17. Chen, L.J.; Dong, B.J.; Liu, W.; Wu, F.; Li, H.; Zhang, T.Y. Failure analysis of corrosion products formed during CO₂ pre-corrosion of X70 and 3Cr steels: Effect of oxygen contamination. *Eng. Fail. Anal.* **2022**, *140*, 106529. [[CrossRef](#)]
18. Kashima, K.; Sugae, K.; Kamimura, T.; Miyuki, H.; Kudo, T. Effect of Chromium Contents on Atmospheric Corrosion of Steel in Chloride Environment. *J. Jpn. Inst. Met. Mater.* **2013**, *77*, 107–113. [[CrossRef](#)]
19. Xu, X.X.; Wu, W.; Li, N.N.; Zhang, L.L.; Wang, Y.; Liu, Z.Y.; Li, X.G. Effect of 0.1 wt% Nb on the microstructure and corrosion fatigue performance of high strength steels. *Corros. Sci.* **2023**, *219*, 111242. [[CrossRef](#)]
20. Ma, H.C.; Liu, Z.Y.; Du, C.W.; Wang, H.R.; Li, X.G.; Zhang, D.W.; Cui, Z.Y. Stress corrosion cracking of E690 steel as a welded joint in a simulated marine atmosphere containing sulphur dioxide. *Corros. Sci.* **2015**, *100*, 627–641. [[CrossRef](#)]
21. Xu, X.X.; Liu, Z.Y.; Zhao, T.L.; Cui, Q.Q.; Zhang, T.Y.; Li, X.G. Corrosion fatigue behavior of Fe-16Mn-0.6C-1.68Al twinning-induced plasticity steel in simulated seawater. *Corros. Sci.* **2021**, *182*, 109282.
22. Wu, W.; Cheng, X.Q.; Zhao, J.B.; Li, X.G. Benefit of the corrosion product film formed on a new weathering steel containing 3% nickel under marine atmosphere in Maldives. *Corros. Sci.* **2020**, *165*, 108416. [[CrossRef](#)]
23. Wu, W.; Dai, Z.Y.; Liu, Z.Y.; Liu, C.; Li, X.G. Synergy of Cu and Sb to enhance the resistance of 3%Ni weathering steel to marine atmospheric corrosion. *Corros. Sci.* **2021**, *183*, 109353. [[CrossRef](#)]
24. Jia, J.H.; Wu, W.; Cheng, X.Q.; Zhao, J.B. Ni-advanced weathering steels in Maldives for two years: Corrosion results of tropical marine field test. *Constr. Build. Mater.* **2020**, *245*, 118463. [[CrossRef](#)]
25. Jia, J.H.; Liu, Z.Y.; Li, X.G.; Du, C.W.; Li, W. Comparative study on the stress corrosion cracking of a new Ni-advanced high strength steel prepared by TMCP, direct quenching, and quenching & tempering. *Mater. Sci. Eng.* **2021**, *825*, 141854.
26. Li, J.K.; Fu, B.G.; Dong, T.S.; Li, G.L.; Liu, Y.Y.; Liu, J.G.; Wang, C.Y.; Cui, W. A new nano-scale rhombic precipitate in the SiC ceramic manufactured by milling-sintering process. *Mater. Charact.* **2023**, *198*, 112731. [[CrossRef](#)]
27. Xu, X.X.; Cheng, H.L.; Wu, W.; Liu, Z.Y.; Li, X.G. Stress corrosion cracking behavior and mechanism of Fe-Mn-Al-C-Ni high specific strength steel in the marine atmospheric environment. *Corros. Sci.* **2021**, *191*, 109760. [[CrossRef](#)]
28. Zhao, Q.H.; Liu, W.; Zhu, Y.C.; Zhang, B.L.; Li, S.Z.; Lu, M.X. Effect of Small Content of Chromium on Wet-Dry Acid Corrosion Behavior of Low Alloy Steel. *Acta Metall. Sin.* **2017**, *30*, 164–175. [[CrossRef](#)]
29. Liu, W.M.; Liu, J.; Pan, H.B.; Cao, F.B.; Wu, Z.J.; Lv, H.H.; Xu, Z.Y. Synergistic effect of Mn, Cu, P with Cr content on the corrosion behavior of weathering steel as a train under the simulated industrial atmosphere. *J. Alloys Compd.* **2020**, *834*, 155095. [[CrossRef](#)]
30. Zhou, Y.; Chen, J.; Xu, Y.; Liu, Z. Effects of Cr, Ni and Cu on the corrosion behavior of low carbon microalloying steel in a Cl-containing environment. *J. Mater. Sci. Technol.* **2013**, *29*, 168–174. [[CrossRef](#)]
31. Sun, M.H.; Pang, Y.J.; Du, C.W.; Li, X.G.; Wu, Y.M. Optimization of Mo on the corrosion resistance of Cr-advanced weathering steel designed for tropical marine atmosphere. *Constr. Build. Mater.* **2021**, *302*, 124346.
32. Sun, M.H.; Du, C.W.; Liu, Z.Y.; Liu, C.; Li, X.G.; Wu, Y.M. Fundamental understanding on the effect of Cr on corrosion resistance of weathering steel in simulated tropical marine atmosphere. *Corros. Sci.* **2021**, *186*, 109427. [[CrossRef](#)]

Disclaimer/Publisher’s Note: The statements, opinions and data contained in all publications are solely those of the individual author(s) and contributor(s) and not of MDPI and/or the editor(s). MDPI and/or the editor(s) disclaim responsibility for any injury to people or property resulting from any ideas, methods, instructions or products referred to in the content.